

Porous Superhydrophobic Membranes: Hydrodynamic Anomaly in Oscillating Flows

S. Rajauria^{1,2}, O. Ozsun³, J. Lawall⁴, V. Yakhot³, and K. L. Ekinci³

¹Center for Nanoscale Science and Technology, National Institute of Standards and Technology, Gaithersburg, Maryland 20899, USA.

²Maryland NanoCenter, University of Maryland, College Park, MD 20742, USA.

³Department of Mechanical Engineering, Boston University, Boston, Massachusetts 02215, USA. and

⁴Atomic Physics Division, National Institute of Standards and Technology, Gaithersburg, Maryland 20899, USA.*

(Dated: March 25, 2025)

We have fabricated and characterized a novel superhydrophobic system, a mesh-like porous superhydrophobic membrane with solid area fraction Φ_s , which can maintain intimate contact with outside air and water reservoirs simultaneously. Oscillatory hydrodynamic measurements on porous superhydrophobic membranes as a function of Φ_s reveal surprising effects. The hydrodynamic mass oscillating in-phase with the membranes stays constant for $0.9 \leq \Phi_s \leq 1$, but drops precipitously for $\Phi_s < 0.9$. The viscous friction shows a similar drop after a slow initial decrease proportional to Φ_s . We attribute these effects to the percolation of a stable Knudsen layer of air at the interface.

To completely describe the flow of a viscous fluid past a solid body, one must solve the Navier-Stokes equations inside the fluid subject to boundary conditions on the solid surface [1]. These boundary conditions cannot be obtained from hydrodynamics, but emerge from the microscopic interactions of fluid particles with the surface. Consequently, they are not universal. It is well-established, for instance, that the commonly-assumed no-slip boundary condition can be violated [2] on both hydrophobic[3–6] and superhydrophobic surfaces [7–10], where the water flows partially on an air cushion instead of the solid. The consequences of a shift in boundary condition from no-slip to partial-slip are vast. Many natural organisms survive simply by virtue of slip [11–13]. Slip flows are poised to impact technology by enabling drag reduction in both laminar [4] and turbulent flows [14]. This list goes on.

On a conventional superhydrophobic surface[15], hydrophobicity combined with microscopic roughness causes the water surface to remain suspended above the solid tips, with mostly trapped air underneath [16, 17]. Since the flow is on a composite surface made up of solid and air, one solves the Navier-Stokes equations subject to no-slip on the solid elements and slip at the water-air interface [2]. Thus, in a first pass analysis, viscous friction force on a superhydrophobic surface is proportional to the wet solid area, Φ_s [18]. In this manuscript, we show that flow on a porous superhydrophobic membrane deviates from the above picture. Oscillatory measurements [19] of viscous friction force and hydrodynamic mass both suggest that a stable Knudsen layer of gas percolates on the membrane, changing the boundary condition. This is because the porous superhydrophobic membrane structure enables the surrounding air to move ballistically to the interface with little resistance — in contrast to a conventional superhydrophobic surface, where trapped gas pockets are diffusively connected to a gas reservoir through macroscopic distances.

The novel system under study shown in Fig. 1 is a

tension-dominated porous silicon nitride membrane made hydrophobic by silanization. The membrane has a (nominal) macroscopic area of $a \times a = 600 \mu\text{m} \times 600 \mu\text{m}$ and a nanoscale thickness of $t_s = 200 \text{ nm}$. A matrix of identical square pores with dimensions $l_g \times l_g = 10 \mu\text{m} \times 10 \mu\text{m}$ are lithographically etched in the membrane. The pitch is $l_g + l_s$, where l_s is the width of the solid strips in between the pores, as shown in Fig. 1(b). This results in a solid area fraction $\Phi_s = 1 - \frac{l_g^2}{(l_g + l_s)^2}$. When a drop of water is placed on the porous membrane, it is supported by a composite surface of solid and gas (air); thus, wetting is not favored as shown in Fig. 1(d).

We first characterize the *intrinsic* mechanical properties of this system in vacuum. For a tension dominated square membrane with thickness t_s and side length a , the (angular) frequency of the normal mode (m, n) is given by $\Omega^{mn} = [\frac{\sigma_s \pi^2}{\Phi_s \rho_s t_s a^2} (m^2 + n^2)]^{1/2}$ [20]. Here, σ_s is the tension, ρ_s is the density, and m and n are two integers corresponding to the number of antinodes along the two directions parallel to the membrane sides. The *in vacuo* mode frequencies $\frac{\Omega^{mn}}{2\pi}$ of a $\Phi_s = 0.34$ membrane are shown in Fig. 1(e). Here, the membrane is excited by a piezoelectric-shaker and its resonances are detected using a Michelson interferometer at a pressure of 10^{-2} Pa. The data confirm that the tension-dominated membrane approximation holds well, even for a membrane with a very small solid fraction. Given that the modes are well-separated in frequency, each mode (m, n) can be modeled as a damped harmonic oscillator with effective mass $M_s = \frac{\rho_s \Phi_s t_s a^2}{4}$ and stiffness $K_s = \frac{\sigma_s \pi^2}{4} (m^2 + n^2)$. Relevant mechanical parameters for the fundamental modes of all our membranes are displayed in Table 1.

We now turn to measurements with water. The measurements are performed using a fluid cell *atop* the membrane as shown in Fig. 2(a). The porous membrane does *not* leak but supports intimate and continuous contact with both the water reservoir above and the gas reservoir (ambient atmosphere) below. Using a heterodyne

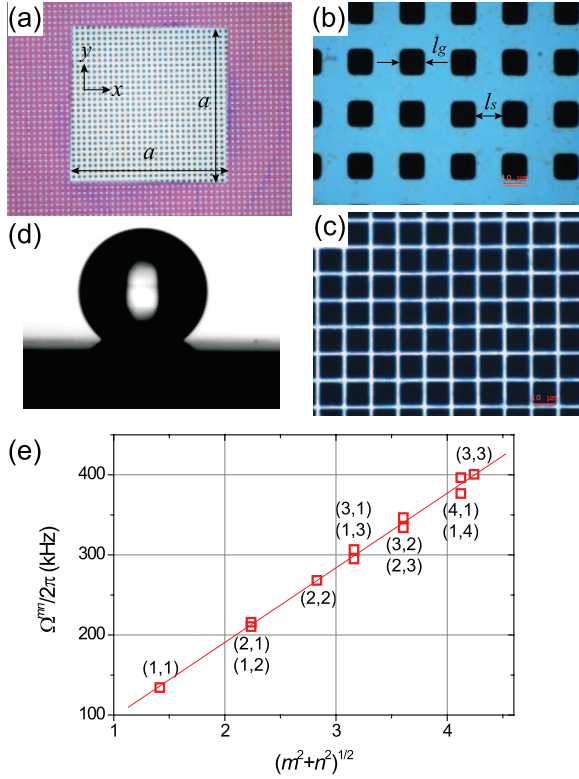


FIG. 1: (a) Top view of a porous membrane chip ($a \times a = 600 \mu\text{m} \times 600 \mu\text{m}$). (b), (c) Optical micrographs of $\Phi_s = 0.78$ and 0.34 membranes, respectively. (d) A drop of water placed on a larger membrane ($a \times a = 2 \text{ mm} \times 2 \text{ mm}$ and $\Phi_s = 0.48$) showing the superhydrophobicity of the surface. (e) Vacuum mechanical resonances of a square porous membrane with $\Phi_s = 0.34$. Nearly-degenerate modes (m, n) and (n, m) are observed when $m \neq n$. Single standard deviations in the data are smaller than the symbols.

TABLE I: Mechanical properties for the fundamental mode of the porous membranes.

Φ_s	$\Omega^{11}/2\pi$ (kHz)	K_s (N/m)	M_s (10^{-12} kg)
1	235	134	61.2
0.96	233	126	58.7
0.88	223	104.7	53.8
0.82	208	67.6	50.2
0.78	142	38.1	47.7
0.65	159	39.2	39.8
0.48	106	12.9	29.4
0.34	134	14.2	21.1

Michelson interferometer (with a displacement sensitivity of $100 \text{ fmHz}^{-0.5}$ around 10 kHz with $85 \mu\text{W}$ incident on the photodetector), we have measured the thermal-noise spectra of all the membranes in their fundamental modes. Fig. 2(b) shows the noise spectra measured at the center of three membranes with different Φ_s . In order to confirm that we are working with the (1,1) mode (fun-

damental mode), we have scanned the optical spot along the x and y directions and obtained mode shapes, such as the one shown in the inset of Fig. 2(b). Since we exclusively study the hydrodynamic properties of the (1,1) mode in the remainder of the manuscript, we henceforth drop the superscript 11. The top data trace in Fig. 3(c) shows all the fundamental resonance frequencies in vacuum, $\frac{\Omega}{2\pi}$, extracted by driving the membranes linearly. Thermal spectra with water atop the membranes have provided the resonance frequencies $\frac{\Omega_w}{2\pi}$ and linewidths $\frac{\gamma}{2\pi}$ [bottom trace in Fig. 2(c)].

We first provide a general discussion of the fluid dynamics encountered in our system. We consider the out-of-plane (broadside) oscillations of a rigid square ($a \times a$) plate *immersed* in a viscous fluid. We take the plate velocity as the real part of the complex exponential, $\mathbf{u}_s = \Re \{U_s e^{i\omega t} \hat{\mathbf{z}}\}$, with amplitude U_s . Adopting the no-slip boundary condition, we find the magnitude of the fluidic force $F_f \hat{\mathbf{z}}$ on the plate in the high-frequency limit as [22]

$$F_f \approx \Re \left\{ A \frac{\mu_f a^2}{\delta} u_s e^{i\phi} + M_f \frac{du_s}{dt} \right\}, \quad (1)$$

with $\phi \approx \frac{\pi}{4}$ and $A \sim 20$. The viscous boundary layer thickness, $\delta = \sqrt{\frac{2\mu_f}{\rho_f \omega}}$, depends on the dynamic viscosity μ_f and density ρ_f of the fluid. M_f is the so-called added or hydrodynamic mass, well-known from the potential theory of flow around an accelerating solid body. Consequences of Equation (1) are as follows. The viscous energy dissipation is due to a flow tangential to the solid plate, expressed by the first term on the right hand side. Being proportional to μ_f , the dissipation provides a widely-used probe of the fluid-solid interaction near the boundary. The second term does *not* contribute to dissipation since $u_s \frac{du_s}{dt}$ integrated over a cycle is zero. However, this term provides an independent probe of the fluid properties (near the solid) through the fluid density ρ_f . To see this, we write $M_f = \rho_f V_f$, where V_f stands for the volume of fluid displaced by plate motion and depends *only* upon geometry. Indeed, it will be shown below that, in our system, the changes in the nature of the fluid near the solid boundary results in changes in both M_f and the dissipation.

Returning to the membrane oscillations, we make a one-dimensional harmonic oscillator approximation for the fundamental mode with position z_s and velocity $\mathbf{u}_s = \dot{z}_s \hat{\mathbf{z}}$. We assume that u_s is nearly sinusoidal because all the membrane resonators have quality factors $Q \gtrsim 20$ and the thermal drive force F_{th} has a white spectrum: $u_s \approx \Re \{U_s e^{i\Omega_w t}\}$. Given that the intrinsic dissipation of the membrane is very small, we write $M_s \dot{u}_s \approx F_f + F_e$, where $F_e = -K_s z_s$ is the elastic spring force due to the mode spring constant and F_f is the fluidic force acting on the mode [see Eq. (1)]. Based on these considerations,

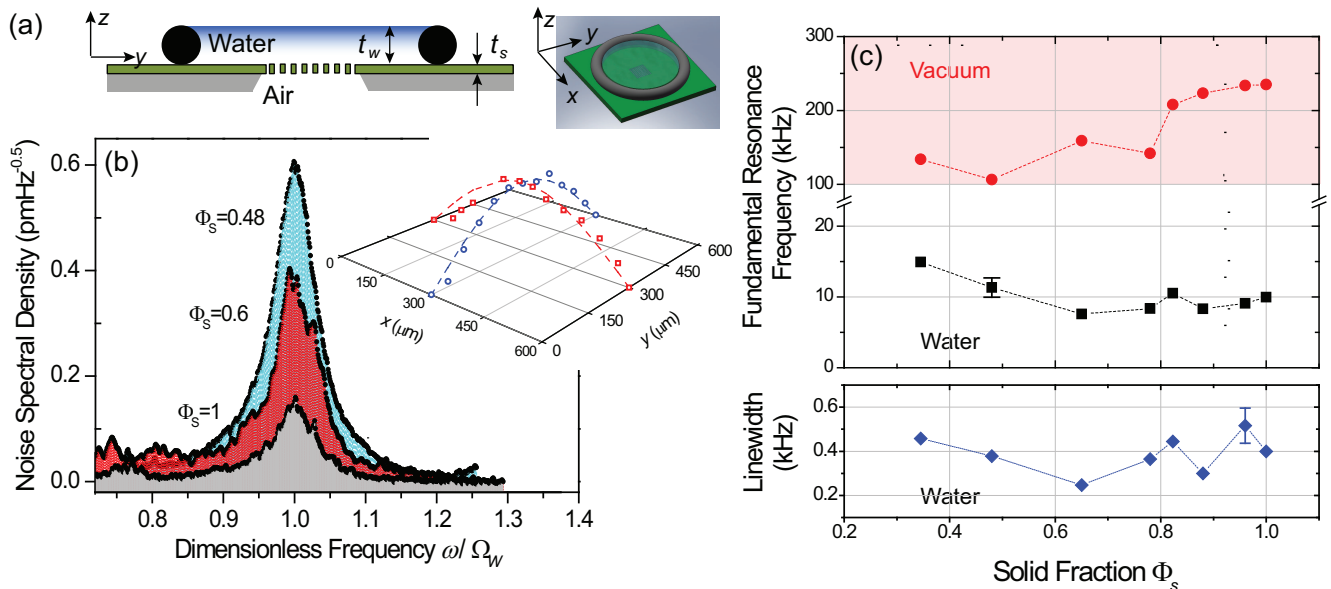


FIG. 2: (a) Schematic of the measurement cell in cross-sectional and isometric views. The cell is filled with water and is placed on top of the membrane chip, while a heterodyne Michelson interferometer probes the motion from below. (b) Thermal noise spectra of the fundamental mode, $(m, n) = (1, 1)$, for three membranes with $\Phi_s = 0.48, 0.6$ and 1 . The frequency axis is normalized with the respective resonance frequencies in water. The inset shows the shape of the fundamental mode for the $\Phi_s = 0.6$ membrane. (c) Fundamental-mode resonance frequencies in vacuum and with water atop, and linewidths $\gamma/2\pi$ with water atop. Error bars represent the associated single standard deviations and are only shown when larger than the symbols.

one can write a complex linear response function for the system as [23] $G(\omega) \approx \frac{1}{K_s - (M_s + M_w^z)\omega^2 + i\alpha\omega}$. The effect of the fluid is embedded in two measurable parameters: the added water mass M_w^z and the friction coefficient α [24].

From the data presented in Fig. 2 and Table 1, we first extract the added mass: $M_w^z \approx M_s \frac{\Omega^2}{\Omega_w^2} = \frac{\Phi_s \rho_s t_s a^2 \Omega^2}{4\Omega_w^2}$ [25], given that $M_s \ll M_w^z$. Figure 3(a) shows M_w^z as a function of Φ_s . Note the two separate regions in Fig. 3(a) with a transition around $\Phi_s \approx 0.9$. In order to estimate M_w^z , we first emphasize that our resonator is *not* immersed in water [see Fig. 2(a)] — unlike in a typical set up. There is a water layer of thickness $t_w = 2.4$ mm and density ρ_w atop the membrane, but the backside is exposed to atmosphere. The dominant hydrodynamic mass contribution comes from the the entire water layer moving in-phase with the membrane oscillations in the z direction. This provides $M_w^z \approx \frac{\rho_w t_w a^2}{4} \approx 2 \times 10^{-7}$ kg [dotted line segment in Fig. 3(a)]. This estimate is in agreement with the data of Fig. 3(a), but *only* in the region $0.9 \leq \Phi_s \leq 1$. Furthermore, in this region, reducing t_w to approximately 1.2 mm results in a frequency increase by a factor of 1.2, close to the factor $\sqrt{2}$ expected from this simple consideration. The shear-induced added masses, M_w^x and M_w^y , are negligibly small because $\delta \approx 6 \mu\text{m} \ll t_w$ when $\Phi_s \approx 1$. For $\Phi_s \lesssim 0.9$, there is a significant deviation from this simple model: the measured hydrodynamic mass shows a rather fast

decrease, eventually by a factor of 23.

The upper, slowly increasing trace in Fig. 3(b) is the cycle-averaged viscous force on the membrane, $\frac{A\mu_w a^2 \Phi_s U_s}{2\pi^2 \delta}$, predicted using the plate model of Eq. (1) and taking the membrane mode-shape into account. Here, μ_w is the dynamic viscosity of water; $\frac{A}{2\pi^2} \sim 1$; $U_s^2 \approx 2\pi^2 \Omega_w^2 \langle z^2 \rangle$, $\langle z^2 \rangle^{1/2}$ being the thermal amplitude of the membrane found from the integral of the measured displacement noise spectral density. It is important to note that, as Φ_s becomes smaller, U_s increases. This is because the stiffness K_s decreases (see Table 1) while the average thermal drive force remains unchanged and Ω_w changes very slowly. In the calculated plate model, the decrease in the wet area, $a^2 \Phi_s$, appears to be off-set by this increase in U_s , thus resulting in a net increase in the drag force as Φ_s decreases. The *measured* cycle-averaged friction force, $\alpha U_s \approx M_w^z \gamma U_s$, shows a surprising deviation from the plate model (lower trace in Fig. 3b). As in added mass, the plate prediction agrees with the experiments when $\Phi_s \approx 1$. However, for $\Phi_s \lesssim 0.9$, the drag force decreases rapidly, attaining a value an order of magnitude smaller than the plate prediction at $\Phi_s = 0.34$.

The drag reduction on the porous membranes can be better assessed, if one considers the drag force per unit velocity: this is the friction coefficient α . Figure 3(c) shows the predicted and experimentally-obtained normalized friction coefficients, $\frac{\alpha(\Phi_s)}{\alpha(1)}$. The predicted value

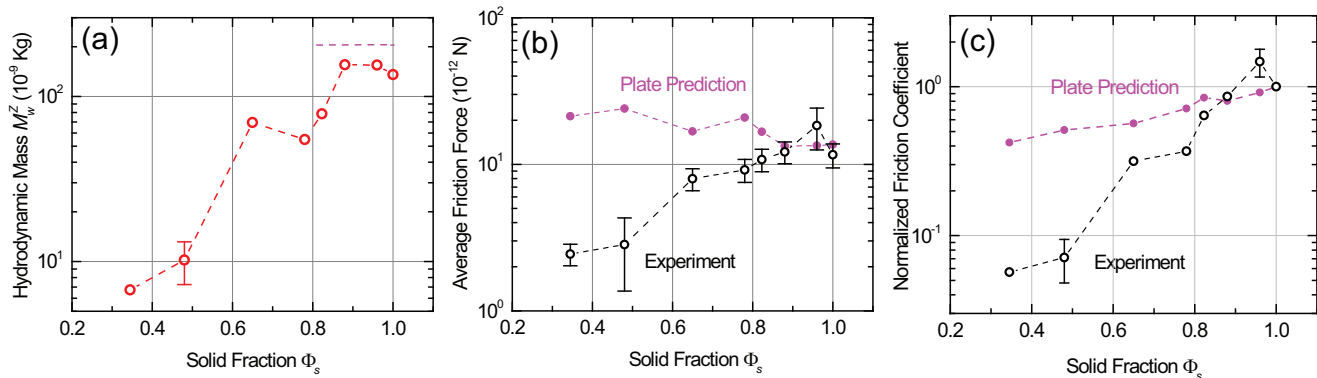


FIG. 3: (a) Measured M_w^z as a function of Φ_s . The line segment is the hydrodynamic mass of the entire water layer. (b) Average friction force and (c) the normalized friction coefficient. The plate prediction is calculated from Eq. (1) using experimental velocities and frequencies where needed. The normalized friction coefficient for the plate model is $\approx \Phi_s$. Error bars represent the associated single standard deviations and are only shown when larger than the symbols.

is proportional to Φ_s since the system behaves as a plate, but with a reduced solid area. The experimental values are given by $\alpha \approx M_w^z \gamma$. The data show that the drag force for a given velocity can be reduced by a factor of 18, if one goes from a complete membrane ($\Phi_s = 1$) to $\Phi_s = 0.34$, i.e., $\alpha(0.34) \approx \alpha(1)/18$.

Given that the membranes do not leak and the hydrodynamic mass M_w^z is constant for $0.9 \leq \Phi_s \leq 1$, we conclude that the presence of the air reservoir does not affect the flow in this interval. The agreement between the predicted and measured friction forces in the same interval provides more support for this conclusion. The significant deviation in the measured flow parameters from the plate model for $\Phi_s \lesssim 0.9$, however, suggests that the flow changes around $\Phi_s \approx 0.9$. The new feature of our system is its openness to air at atmospheric pressure. The membrane thickness, $t_s = 200$ nm, is close to the mean-free-path of air, $\lambda_g \approx 60$ nm. This enables the surrounding air to move through the membrane pores with little or no resistance. The dramatic decrease in M_w^z for $\Phi_s < 0.9$ can be attributed to a percolation transition: air bubbles localized within the well-defined pores begin to coalesce as Φ_s is decreased, eventually resulting in a complete gas layer, which separates the solid strips from the water surface.

Assuming a complete Knudsen layer at the interface, we can assess the friction reduction on a porous membrane with small Φ_s . A one-dimensional model will suffice. We consider a large porous plate oscillating in its plane with velocity, $\Re\{U_s \hat{x} e^{i\Omega_w t}\}$, under water with a Knudsen air layer in between the plate and the water. The velocity field inside the water is $\Re\{U_w \hat{x} e^{-\frac{z}{\delta} + i(\Omega_w t - \frac{z}{\delta})}\}$ and $U_w \neq U_s$. Since the stress is a continuous function of coordinate at the interface ($z \approx 0$), $\frac{\mu_w U_w}{\delta} \sim \frac{\rho_g U_s \Phi_s u_{th}}{6}$. Here, $U_s \Phi_s$ and u_{th} are respectively the average hydrodynamic velocity and the

thermal velocity of air molecules; ρ_g is the density of air. The factor $1/6$ accounts for the fraction of molecules traveling in the $+z$ direction. Using the parameters available, we derive $\frac{U_s}{U_w} \sim \frac{3}{\Phi_s}$. The slip length, $\lambda \sim \frac{\mu_w}{\rho_g u_{th} \Phi_s}$, thus emerges as $6 \mu\text{m}$ at $\Phi_s = 0.34$.

Our results might be relevant to applications. Unlike air bubbles on a hydrophobic surface [21], the air layer in our system is stable against diffusion into the water because of the constant and resistance-free influx from the air reservoir. Assuming that thin porous pipes of macroscopic dimensions can be manufactured, significant drag reduction in could be achieved. Several puzzling phenomena in bio-fluid-dynamics, including transport through and over biological membranes, and propulsion over the water surface, may be related to the interesting physics observed here [12, 13].

The authors thank L. Chen and G. Holland for technical assistance, and J. A. Liddle and V. Aksyuk for fruitful discussions. Support from the US NSF (through grants ECCS-0643178, CBET-0755927, and CMMI-0970071) is acknowledged.

* e-mail:ekinci@bu.edu

- [1] L.D. Landau, and E.M. Lifshitz, *Fluid Mechanics* (Butterworth-Heinemann, Oxford, 1987), 2nd ed.
- [2] E. Lauga, M. Brenner, and H.A. Stone, *Handbook of Experimental Fluid Mechanics*, edited by C. Tropea, A. L. Yarin, and J. F. Foss. Springer-Verlag, Berlin, 2007.
- [3] O.I. Vinogradova, *Langmuir* **11**, 22132220 (1995).
- [4] D.C. Tretheway and C.D. Meinhart, *Phys. Fluids* **16**, 15091515 (2004).
- [5] J.W.G. Tyrrell and P. Attard, *Phys. Rev. Lett.* **87**, 176104 (2001).
- [6] X.H. Zhang, A. Khan, and W.A. Ducker, *Phys. Rev. Lett.* **98**, 136101 (2007).

- [7] P. Joseph et al., *Phys. Rev. Lett.* **97**, 156104 (2006).
- [8] C.H. Choi and C.J. Kim, *Phys. Rev. Lett.* **96**, 066001 (2006).
- [9] C. Cottin-Bizonne et al., *Nat. Mat.* **2**, 237-240 (2003).
- [10] A.M.J. Davis and E. Lauga, *Phys. Fluids* **21**, 113101 (2009).
- [11] C. Neinhuis and W. Barthlott, *Annals of Botany* **79**, 667-677 (1997).
- [12] J.W.M. Bush, D.L. Hu, and M. Prakash, *Advances in Insect Physiology* Volume 34, 2007, Pages 117-192.
- [13] X. Gao, and L. Jiang, *Nature* **432**, 36 (2004).
- [14] R.J. Daniello, N.E. Waterhouse, and J.P. Rothstein, *Phys. Fluids* **21**, 085103 (2009).
- [15] P.G. de Gennes, F. Brochard-Wyart, and D. Quere, *Capillarity and Wetting Phenomena: Drops, Bubbles, Pearls, Waves* Springer, New-York, 2004.
- [16] M. Miwa et al., *Langmuir* **16**, 57545760 (2000).
- [17] J. Bico, C. Tordeux, and D. Quéré, *Europhys. Lett.* **55**, 214-220 (2001).
- [18] C. Ybert et al., *Phys. Fluids* **19**, 123601 (2007).
- [19] K.L. Ekinici et al., *Lab Chip* **10**, 30133025 (2010).
- [20] S. Timoshenko, D.H. Young, and W. Weaver, Jr., *Vibration Problems in Engineering* (John Wiley and Sons, 1974).
- [21] M.P. Brenner and D. Lohse, *Phys. Rev. Lett.* **101**, 214505 (2008).
- [22] W. Zhang and H.A. Stone, *J. of Fl. Mech.* **367**, 329-358 (1998).
- [23] M.R. Paul, M.T. Clark, and M.C. Cross, *Nanotechnology* **17**, 4502-4513, (2006).
- [24] F. Reif, *Fundamentals of Statistical and Thermal Physics* (New York, NY: McGraw-Hill, 1965).
- [25] A. Maali et al., *J. Appl. Phys.* **97**, 074907 (2005)